

# Morphology Evolution and Improved Electrochemical Properties of LiFePO<sub>4</sub> Cathode Materials for Li-ion Batteries

Erchao Meng<sup>\*</sup>, Jianlin Sun, Ying Huang, Huajie Tang

National Demonstration Center for Experimental Materials Education, School of Materials Science and Engineering, University of Science and Technology Beijing, Beijing 100083, China

\*E-mail: [mengec@ustb.edu.cn](mailto:mengec@ustb.edu.cn)

Received: 29 September 2022 / Accepted: 6 November 2022 / Published: 17 November 2022

---

LiFePO<sub>4</sub> powders with different sizes and shapes were successfully synthesized in water, ethylene glycol, and mixed water/ethylene glycol solvents. The morphological evolution of LiFePO<sub>4</sub> crystals from micrometer-sized bulky particles to nanorods was easily achieved by varying the water-to-ethylene glycol volume ratio. The morphological evolution process and formation mechanism were investigated. Electrochemical measurements showed that the charge transport and the diffusion rate of Li ions significantly improved with the structural evolution. The initial discharge capacity at 0.1 C was increased from 61 mAh·g<sup>-1</sup> for micrometer-sized bulky particles to 164 mAh·g<sup>-1</sup> for nanorods. Furthermore, the LiFePO<sub>4</sub> nanorods exhibited a discharge capacity of about 120 mAh·g<sup>-1</sup> at 20 °C and an excellent rate capability at high discharge rates.

---

**Keywords:** Lithium-ion batteries; LiFePO<sub>4</sub>; cathodes; crystal growth; structural control; electrochemical performance.

## 1. INTRODUCTION

Owing to its excellent reversibility, good thermal and chemical stability, low cost, and environmentally friendliness, LiFePO<sub>4</sub> is considered a relatively good cathode material for Li-ion batteries, and it was applied in energy storage facilities and electric vehicles [1-4], with expectations to a broader market shortly [5].

However, low Li-ion diffusion rate and poor electronic conductivity severely restrict its electrochemical performance, especially rate capability [6]. To improve these shortcomings, researchers applied different strategies, including doping [7], morphology control [5] and interfacial modification [8]. We also reported some effective approaches to improve the electrochemical properties of LiFePO<sub>4</sub> cathodes [6, 9, 10], demonstrating that the electrochemical properties can be significantly improved by reducing the size and/or controlling the morphology of LiFePO<sub>4</sub> [11-15]. Using ethylene glycol (EG) as

a stabilizer or solvent to control the crystal growth of  $\text{LiFePO}_4$  crystals was reported as an effective strategy [12, 16]. However, further studies are needed to clarify the influence of the amount of EG in hydrothermal/solvothermal synthesis on the morphological evolution of  $\text{LiFePO}_4$  crystals.

In this work, we report that the size and shape of  $\text{LiFePO}_4$  crystals can be gradually modified from micrometer-sized particles to nanorods by simply tuning the water-to-EG volume ratio in the solvent. The morphological evolution process is discussed in detail. Finally, the electrochemical properties of  $\text{LiFePO}_4$  with different morphologies are investigated.

## 2. EXPERIMENTAL

### 2.1 Synthesis of $\text{LiFePO}_4$ cathode materials

All chemical reagents were of analytical grade.  $\text{LiFePO}_4$  cathode materials were synthesized using a solvent made of water and ethylene glycol mixed in a volume ratio of 4:0, 3:1, 2:2, 1:3, and 0:4. The corresponding products were named LFP-1, LFP-2, LFP-3, LFP-4, and LFP-5, respectively. The molar ratio of Li: Fe: P was 2.5:1:1.  $\text{FeSO}_4 \cdot 7\text{H}_2\text{O}$  and  $\text{H}_3\text{PO}_4$  were dissolved in 20 ml of mixed solvent as solution A, and  $\text{LiOH} \cdot \text{H}_2\text{O}$  was dissolved in another 20 ml of mixed solvent as solution B. Then, solution B was dropwise added into solution A under magnetic stirring. The mixtures were transferred into a 50-ml Teflon-lined stainless-steel autoclave and kept at 180 °C for 4 h. After cooling to room temperature, the resulting solid products were washed several times using water and ethanol and dried at 60 °C for 12 h. The obtained  $\text{LiFePO}_4$  products were carbon-coated through uniform mixing with about 20 wt.% glucose and then heated at 650 °C for 3 h in an argon atmosphere.

### 2.2 Electrochemical characterization

The phase and crystalline structures of the as-prepared products were characterized using XRD (Bruker D8). The morphological characteristics of the products were examined using FESEM (JEOL JSM-7001F) and TEM (JEOL JEM-2100F), and the chemical and structural characteristics were assessed using XPS (Thermo Fisher Scientific) and Raman (HORIBA Scientific LabRAM HR Raman spectrometer) spectroscopy, respectively.

### 2.3 Electrochemical measurements

The  $\text{LiFePO}_4$  cathode materials were used to assemble CR2016 coin-type cells via mixing the active material/acetylene black/poly (vinylidene fluoride) (PVDF) with a weight ratio of 80:15:5. The detailed fabrication process of working electrodes was reported in our previous work [6]. Metallic Li foil, 1 M  $\text{LiPF}_6$  in ethylene carbonate/dimethyl carbonate (1:1 v/v), and polypropylene micro-porous films (Celgard 2300) were used as a counter electrode, an electrolyte, and separators, respectively. The CR2016 cells were assembled in a glove box. The mass loading range of the active materials was 2.0 - 2.5  $\text{mg} \cdot \text{cm}^{-2}$ .

Galvanostatic charge/discharge experiments were carried out using a charge/discharge instrument (Xinwei CT3008) in the voltage range of 2.5 - 4.2 V (vs. Li/Li<sup>+</sup>). Electrochemical impedance spectroscopy (EIS) and cyclic voltammetry (CV) measurements were performed using an electrochemical workstation (Chenhua, CHI660E). Furthermore, the CV measurements were performed using fresh cells at a scanning rate of 0.1 mV·s<sup>-1</sup> between 2.5 and 4.2 V. The EIS measurements were carried out using fresh cells in the frequency range from 100 kHz to 10 mHz with an applied amplitude of 5 mV.

### 3. RESULTS AND DISCUSSION

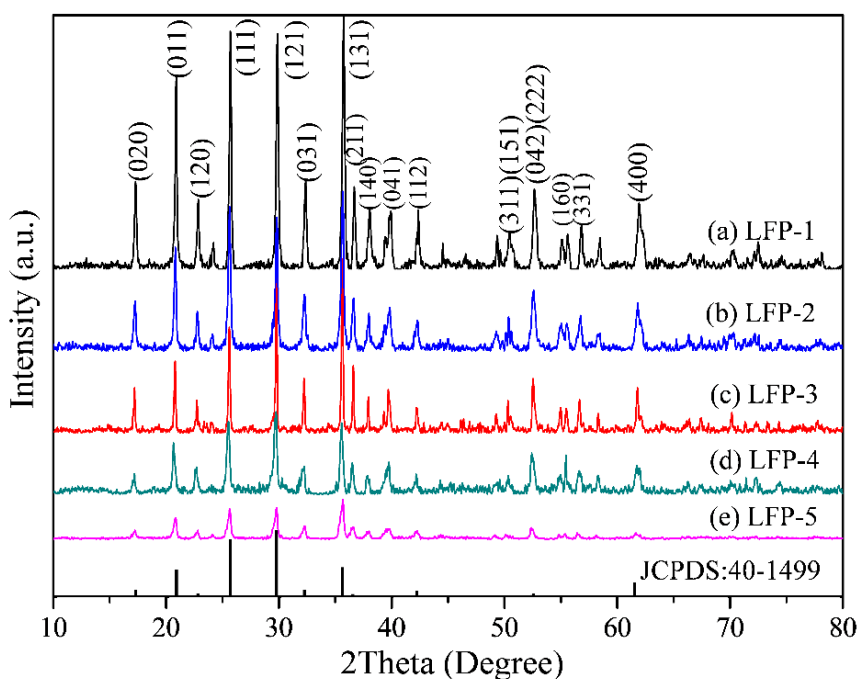


**Figure 1.** XRD patterns of the LiFePO<sub>4</sub> products.

XRD patterns shown in Figure 1 show almost the same major diffraction for all LiFePO<sub>4</sub> products, and all the diffraction peaks could be indexed to standard crystalline orthorhombic LiFePO<sub>4</sub> (PDF# 40-1499) without detectable impurities. The results indicate that LiFePO<sub>4</sub> crystals are successfully synthesized using solvents with different water-to-EG volume ratio. The solvent composition exhibits no obvious effect on the phase and purity of LiFePO<sub>4</sub> products. It is worth noting that the diffraction peak intensity decreases, also exhibiting peak broadening in the direction from LFP-1 to LFP-5, which suggests that the crystallinity and size of LiFePO<sub>4</sub> particles gradually decrease [17].

The structural characteristics of the as-prepared LiFePO<sub>4</sub> products were characterized by FESEM and TEM. As shown in Figure 2, LiFePO<sub>4</sub> crystals with different morphologies are successfully synthesized in the water/EG solvent, and the size and shape of LiFePO<sub>4</sub> crystals depend on the volume ratio of water to EG. High-magnification FE-SEM and TEM images show that when the volume ratio of

water to EG is 4:0, 3:1, 2:2, 1:3, and 0:4, the corresponding  $\text{LiFePO}_4$  products exhibit micrometer-sized bulky particles, then their morphology changes to pillow-like, candy-like, nanometer-sized spindle shapes, and finally, nanorods, respectively. The  $\text{LiFePO}_4$  nanorods exhibit uniform and completely crystalline particles, while the other four samples exhibit a hierarchical morphology assembled by micrometer- or nanometer-sized crystal particles. It can be observed that the size and shape evolve from micrometer-sized bulky particles to nanorods with the volume ratio of EG in the used solvent.

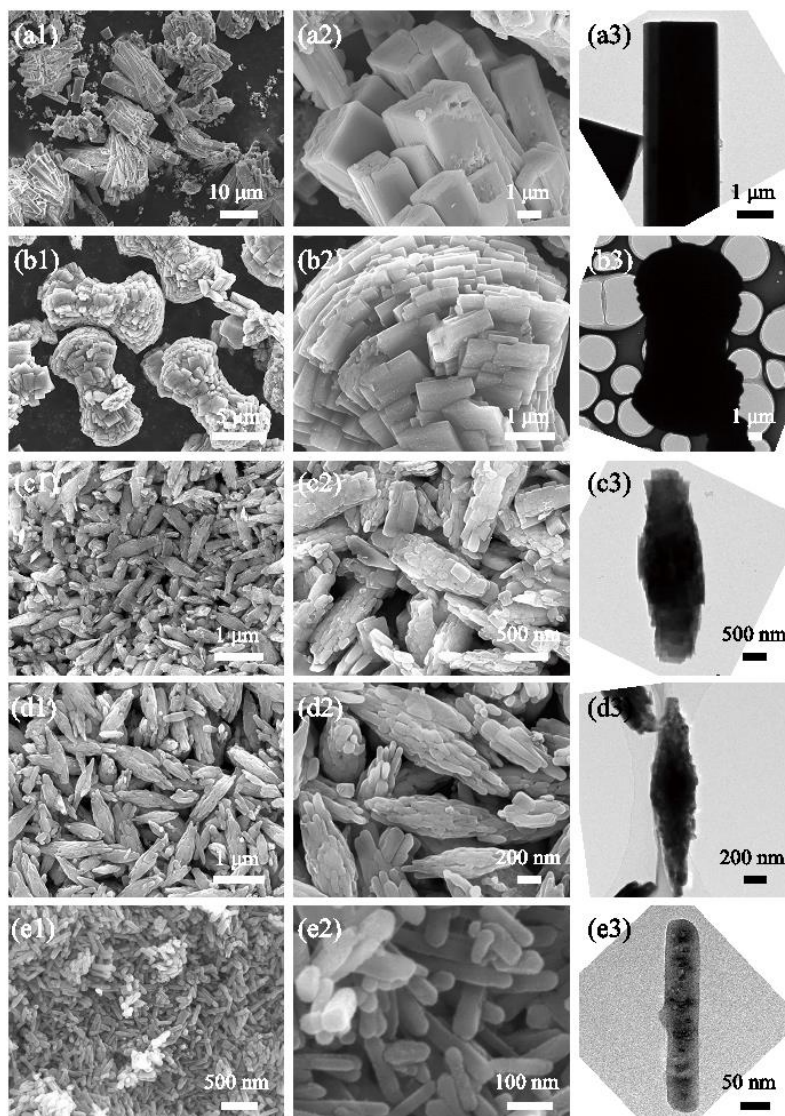


**Figure 2.** FESEM and TEM images of (a1-a2, a3) LFP-1, (b1-b2, b3) LFP-2, (c1-c2, c3) LFP-3, (d1-d2, d3) LFP-4, and (e1-e2, e3) LFP-5.

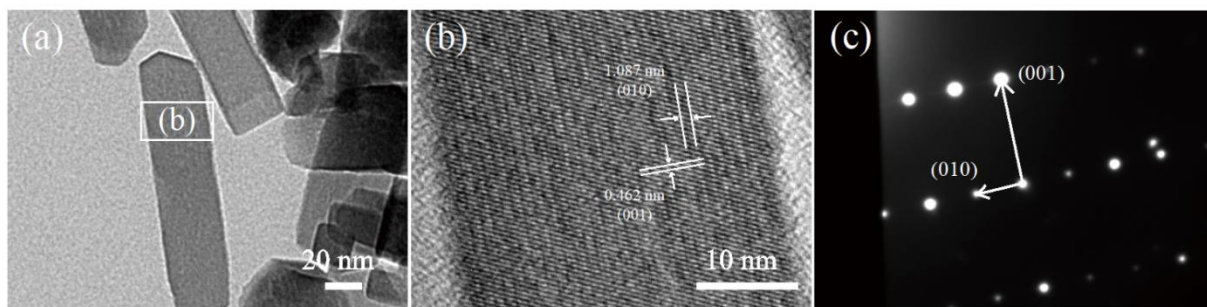


**Figure 3.** TEM, HRTEM and FFT images of the LFP-5 sample.

The  $\text{LiFePO}_4$  nanorods are further characterized by TEM, as shown in Figure 3. HRTEM and FFT images indicate that the  $\text{LiFePO}_4$  nanorods are single crystals, preferentially grown along the [001] direction, with short a- and b-axes, resulting in a shorter Li-ion diffusion path. It is speculated that the  $\text{LiFePO}_4$  crystal growth in the (010) and (100) planes is slowed down due to the adsorption of the organic molecules when introducing EG in the solvent owing to relatively low surface energy and mostly oxygen atoms on these planes [13]. The growth inhibition effect on the (010) and (100) planes enhances with the EG content in the mixed solvent. Thus, the size and shape of  $\text{LiFePO}_4$  can be controlled by increasing the amount of EG in the mixed solvent, yielding  $\text{LiFePO}_4$  nanorods, preferentially grown along the [001] direction, in pure EG solvent.

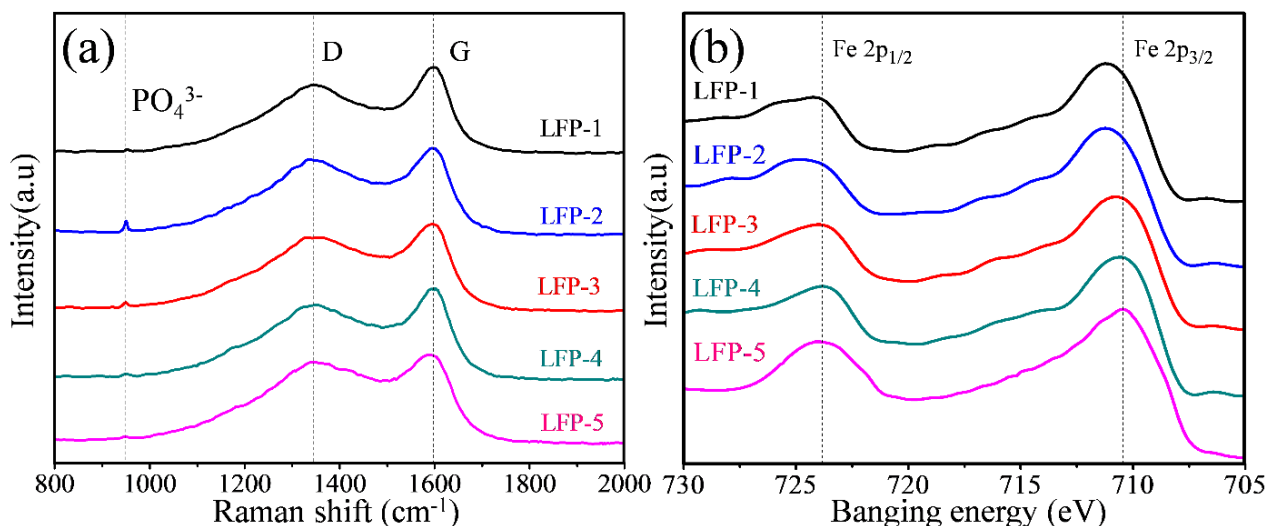


**Figure 4.** (a) Raman spectra and (b) high-resolution  $\text{Fe}2p_{1/2}$  and  $\text{Fe}2p_{3/2}$  XPS spectra of the synthesized  $\text{LiFePO}_4$  products.

Raman characterization was carried out to investigate the structural characteristics of five  $\text{LiFePO}_4$  products, as shown in Figure 4(a). The peaks around  $950\text{ cm}^{-1}$  in the Raman spectra of all samples is attributed to intermolecular stretching motions and antisymmetric stretching modes of the

$\text{PO}_4^{3-}$  [18, 19], suggesting the absence of impurities on the sample surface, and the results are in good agreement with the assignments reported in the literature [20]. The peaks at  $1336\text{ cm}^{-1}$  and  $1595\text{ cm}^{-1}$  correspond to the D and G bands of carbon materials [18]. The G band is related to graphite, while the D band is attributed to the disorder or defects in carbon materials, mainly arising from carbon coating. The results demonstrate that the as-prepared  $\text{LiFePO}_4$  products are successfully carbon-coated.

The valence state of Fe in the as-prepared  $\text{LiFePO}_4$  products was characterized by HR-XPS, and the  $\text{Fe}2p$  spectra of the  $\text{LiFePO}_4$  products are compared in Figure 4(b). The binding energy of  $\text{Fe}2p_{3/2}$  and  $\text{Fe}2p_{1/2}$  of the LFP-5, LFP-4, and LFP-3 samples is at around 710.3 eV and 723.9 eV, respectively, implying that the oxidation state of Fe atoms in these samples is close to  $\text{Fe}^{2+}$ . In addition, the energy separation ( $\Delta E_{\text{Fe}}$ ) is about 13.6 eV, which matches well with the previously reported spectra of  $\text{Fe}^{2+}$  in  $\text{LiFePO}_4$  [19]. However, it is observed that LFP-1 and LFP-2 exhibit the binding energies of  $\text{Fe}2p_{3/2}$  and  $\text{Fe}2p_{1/2}$  closer to  $\text{Fe}^{3+}$ . The XPS results indicate that adding EG in the mixed solvent can also prevent the oxidation of  $\text{Fe}^{2+}$ , acting as a reducing agent in the synthesis process [21].

Furthermore, BET specific surface areas were measured, and they are 1.53, 3.89, 5.58, 14.6, and  $32.02\text{ m}^2\cdot\text{g}^{-1}$  for LFP-1, LFP-2, LFP-3, LFP-4, and LFP-5, respectively. The results demonstrate that the specific surface of  $\text{LiFePO}_4$  is higher for powders with smaller particles size, which is favorable to increasing the actual reaction area and facilitating the transportation of Li ions. The BET results are consistent with the FE-SEM and TEM characterization, suggesting that nanometer-sized  $\text{LiFePO}_4$  exhibits better performance for electrolyte infiltrating and Li-ion diffusion.

Typical initial charge-discharge curves between 2.5 and 4.2 V at 0.1 C ( $17\text{ mA}\cdot\text{g}^{-1}$ ) are shown in Figure 5(a). The initial discharge specific capacities are  $61\text{ mAh}\cdot\text{g}^{-1}$  for LFP-1,  $69\text{ mAh}\cdot\text{g}^{-1}$  for LFP-2,  $106\text{ mAh}\cdot\text{g}^{-1}$  for LFP-3,  $131\text{ mAh}\cdot\text{g}^{-1}$  for LFP-4, and  $164\text{ mAh}\cdot\text{g}^{-1}$  for LFP-5, respectively. Moreover, the voltage differences between the charge and discharge flat plateaus are 89.3, 78.7, 46.2, 27.3, and 8.4 mV for LFP-1, LFP-2, LFP-3, LFP-4, and LFP-5, respectively. The discharge capacity of the corresponding products increases with the EG amount while the polarization decreases.

To evaluate the cycling performance of five  $\text{LiFePO}_4$  products, we performed 100 discharge cycles at 0.1 C, as shown in Figure 5(b). LFP-5 exhibits the highest discharge capacity and excellent cycling stability compared to the other four powders. Furthermore, Figure 5(c) compares the rate performance of five  $\text{LiFePO}_4$  powders at different current densities. All samples were cycled at different current densities from 0.1 to 5 C and then reversed back to 0.1 C. As shown in Figure 5(c), the capacities of all electrodes decrease with the current densities to 5 C, and then, the capacities almost recover to the original values when reversing back to 0.1 C, suggesting that the rate capability of the as-prepared  $\text{LiFePO}_4$  powders is very stable. Furthermore, LFP-5 demonstrates the best rate capability, and its discharge capacities at all discharge rates are the highest. It is worth mentioning that, as shown in Figure 5(d), LFP-5 shows excellent rate capability between 0.2 C and 20 C, still delivering a specific capacity of more than  $120\text{ mAh}\cdot\text{g}^{-1}$  at 20 C. It is confirmed again that the electrical conductivity and Li-ion transport of the as-prepared  $\text{LiFePO}_4$  products are further enhanced by reducing the  $\text{LiFePO}_4$  crystal size to the nanometer scale.

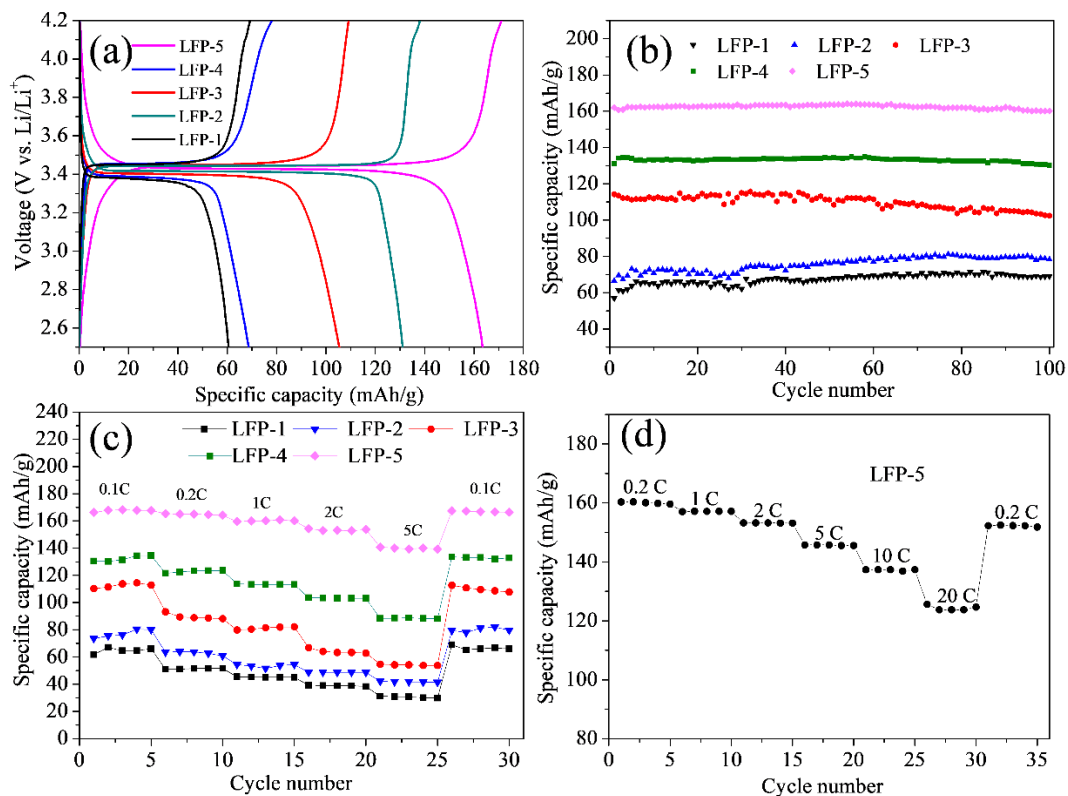


**Figure 5.** (a) Initial charge-discharge profiles, (b) cycling performances, and (c) rate capabilities of the LiFePO<sub>4</sub> products; (d) the rate capability of LFP-5.

**Table 1.** Summary of the electrochemical performance of LiFePO<sub>4</sub> with different morphologies synthesized in the water/EG mixed solvent.

Number	Water/EG	Morphologies	Performance (mAh·g <sup>-1</sup> )	Refs.
1	4:1	Nanobars	114 (0.1 C); 78 (5 C)	Ref. [23]
		Microplates	152 (0.1 C); 116 (5 C)	
		Nanorods	159 (0.1 C); 141 (5 C)	
2	1:1	Nanoparticles	155 (0.1 C); 43 (20 C)	Ref. [24]
		Nanoplates	154 (0.1 C); 83 (20 C)	
3	5:10	Hierarchical Nanostructures	146 (1 C); 135 (4 C)	Ref. [25]
	15:0	Irregular Microparticles	125 (1 C); 105 (4 C)	
4	1:2	Cage-like particles	150 (0.5 C); 120 (10 C)	Ref. [26]
5	1:1	Hollow structured Particles	165.2 (0.1 C); 120.9 (10 C)	Ref. [27]
6	1:15	Nanorods	167 (0.1 C); 127 (10 C)	Ref. [28]
		Large spheres	103 (0.1 C)	
		Rods shape	107 (0.1 C)	
		Large bones shape	110 (0.1 C)	
		Nanodendrites	154 (0.1 C); 141 (5 C)	
8	4:0	Micrometer-sized bulky particles	61 (0.1 C); 31 (5 C)	Our Work
	3:1	Pillow-like particles	69 (0.1 C); 42 (5 C)	
	2:2	Candy-like particles	106 (0.1 C); 54 (5 C)	
	1:3	Nano-sized spindles	131 (0.1 C); 88 (5 C)	
	0:4	Nanorods	164 (0.1 C); 141 (5C); 120 (20 C)	

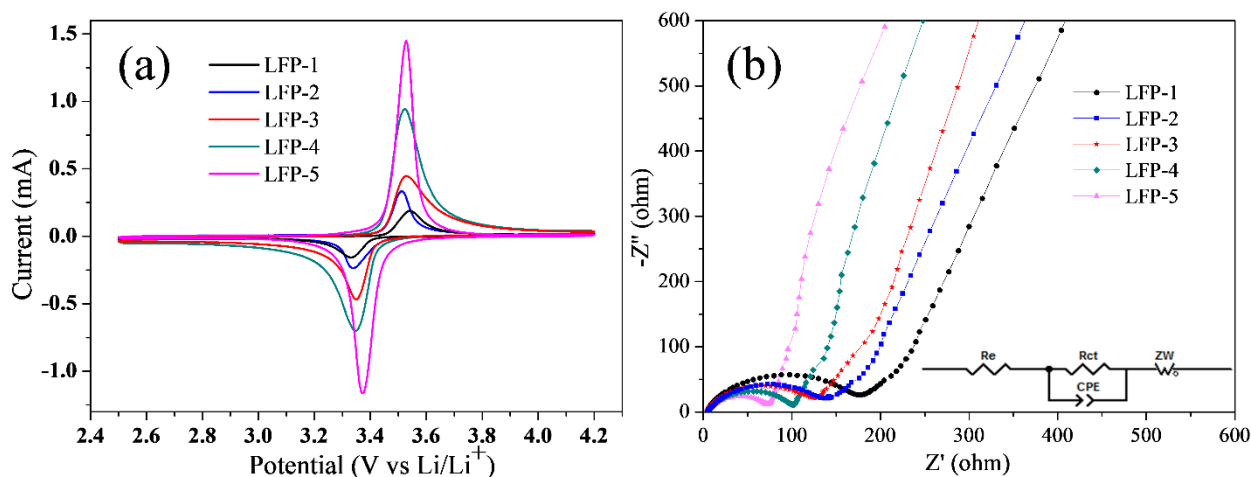


**Figure 6.** (a) CV curves and (b) EIS plots of the LiFePO<sub>4</sub> powders.

Table 1 summarizes the electrochemical performance of LiFePO<sub>4</sub> with different morphologies synthesized in the water/EG mixed solvent. It is found that the nanometer-sized LiFePO<sub>4</sub> powders exhibit excellent electrochemical properties. Especially, the LiFePO<sub>4</sub> nanorods synthesized in our work exhibit the best electrochemical performance among all the LiFePO<sub>4</sub> powders at high discharge rates, e.g., 5 C and 20 C, as summarized in Table 1.

To further investigate the electrochemical kinetics and the improved electrochemical properties of the as-prepared LiFePO<sub>4</sub> products, CV and EIS measurements were carried out using an electrochemical workstation. Figure 6(a) shows the initial CV curves of the five LiFePO<sub>4</sub> powders at a scanning rate of 0.1 mV·s<sup>-1</sup> between 2.5 and 4.2 V. A pair of redox peaks between 3.33 and 3.54 V appear for all LiFePO<sub>4</sub> samples, matching to the Fe<sup>3+</sup>/Fe<sup>2+</sup> redox couple. The potential intervals ( $\Delta V$ ) between the cathodic and anodic peaks are 0.215, 0.184, 0.178, 0.171, and 0.147 V for LFP-1, LFP-2, LFP-3, LFP-4, and LFP-5, respectively. Furthermore, the redox peak profiles gradually become sharper and more symmetric as the particle size of LiFePO<sub>4</sub> decreases. The peak areas in line with the high capacity also become larger [22], suggesting that better reversibility, lower polarization, and higher capacity in the direction from LFP-1 to LFP-5 [10]. Moreover, the improved CV performance also implies lower charge resistance and higher Li-ion diffusion rate, which is confirmed by EIS measurements (see below).

EIS measurements were carried out to investigate the electrochemical kinetic processes of the electrodes using fresh cells in the frequency range from 100 kHz to 10 mHz with an applied amplitude of 5 mV, as shown in Figure 6(b). All LiFePO<sub>4</sub> samples exhibit similar Nyquist plots, with a steep slope in the low-frequency range and a depressed semicircle in the medium-frequency and high-frequency ranges. According to the previous reports, the semicircle is attributed to charge transfer resistance, while the inclined line is associated with the Warburg impedance [6]. EIS can be well understood based on the equivalent circuit, as shown in the inset in Figure 6(b), where R<sub>e</sub>, R<sub>ct</sub>, CPE, and Z<sub>w</sub> correspond to the electrolyte resistance, charge transfer resistance, the constant phase element of the electrode/electrolyte interface, and the Warburg resistance of the Li-ion diffusion process, respectively. The charge transfer resistance (R<sub>ct</sub>) is 176, 148, 130, 101, and 72  $\Omega$  for LFP-1, LFP-2, LFP-3, LFP-4, and LFP-5, respectively, indicating that the lithiation/delithiation kinetics gradually improve as the particle size of

LiFePO<sub>4</sub> samples decreases. In addition, the Li-ion diffusion coefficient ( $D_{\text{Li}}$ ) is determined to be  $0.57 \times 10^{-15}$ ,  $1.08 \times 10^{-15}$ ,  $1.13 \times 10^{-15}$ ,  $1.52 \times 10^{-15}$ , and  $3.10 \times 10^{-15}$  cm<sup>2</sup>·s<sup>-1</sup> for LFP-1, LFP-2, LFP-3, LFP-4, and LFP-5, respectively. The results demonstrate that the charge transport and redox kinetics of the LiFePO<sub>4</sub> cathode material dramatically enhance lead to an excellent electrochemical performance by changing the shape and size of LiFePO<sub>4</sub> crystals by tuning the volume ratio of water to EG in the used solvent.

#### 4. CONCLUSIONS

LiFePO<sub>4</sub> was successfully synthesized in water, EG and mixed water/EG solvents. The size and shape of LiFePO<sub>4</sub> crystals gradually evolved from micrometer-sized bulky particles to nanorods as the volume of EG in the mixed solvent increased. The LiFePO<sub>4</sub> nanorods preferentially grew along the [001] crystal plane, exhibiting short a- and b-axes, which results in shorter Li-ion diffusion paths, enhancing conductivity and Li-ion diffusion. From LFP-1 to LFP-5, i.e., by the size reduction and the change in morphology of particles, the charge transfer resistance reduced from 176 to 72 Ω, and the Li-ion diffusion coefficient increased from  $0.57 \times 10^{-15}$  to  $3.10 \times 10^{-15}$  cm<sup>2</sup>·s<sup>-1</sup>. Meanwhile, the discharge capacity increased from 61 to 164 mAh·g<sup>-1</sup>. Furthermore, LFP-5 exhibited a discharge capacity of about 120 mAh·g<sup>-1</sup> at 20 °C, and an excellent rate capability between 0.2 C and 20 C discharge rates.

#### ACKNOWLEDGEMENTS

This work was financially supported by the Natural Science Foundation of Henan Province (202300410501), the National Key Research and Development Program of China (No. 2021YFB3701305) and the Project of Mass Innovation Space (2020ZCKJ235).

#### References

1. Y.M. Xin, H.Y. Xu, J.H. Ruan, D.C. Li, A.G. Wang, D.S. Sun, *Int. J. Electrochem. Sci.*, 16 (2021) 210655.
2. Y. Ma, T. Li, F. Jiang, Y.Q. Jiang, F.L. Gao, L.Y. Liu, Y.D. Wu, Y. Meng, X.H. Ma, Z.F. Zi, *Int. J. Electrochem. Sci.*, 17 (2022) 220453.
3. M. Zhi, R. Fan, X. Yang, L. Zheng, S. Yue, Q. Liu, Y. He, *J. Energy Storage*, 45 (2022) 103694.
4. S.P. Chen, D. Lv, J. Chen, Y.H. Zhang, F.N. Shi, *Energ Fuel*, 36 (2022) 1232.
5. J. Hu, W. Huang, L. Yang, F. Pan, *Nanoscale*, 12 (2020) 15036.
6. E.C. Meng, M. Zhang, Y. Hu, F.L. Gong, L.S. Zhang, F. Li, *Electrochim. Acta*, 265 (2018) 160.
7. H.H. Zhang, Z.G. Zou, S.C. Zhang, J. Liu, S.L. Zhong, *Int. J. Electrochem. Sci.*, 15 (2020) 12041.
8. S.Q. Zhu, A.M. Huang, Y. Xu, *Int. J. Electrochem. Sci.*, 16 (2021) 210564.
9. Y. Hu, M. Zhang, F.L. Gong, X.M. Qin, Q. Li, E.C. Meng, *Mater. Lett.*, 241 (2019) 72.
10. E.C. Meng, B.H. Jin, Y. Hu, F.L. Gong, Y.H. Zhang, Q.L. Jia, *J. Electrochem. Sci.*, 167 (2020) 160516.
11. Y. Takahashi, A. Kumatani, H. Munakata, H. Inomata, K. Ito, K. Ino, H. Shiku, P.R. Unwin, Y.E. Korchev, K. Kanamura, T. Matsue, *Nat Commun*, 5 (2014) 5450.
12. Z. Li, J. Yang, T. Guang, B. Fan, K. Zhu, X. Wang, *Small Methods*, 5 (2021) 2100193.
13. A.B. Kanagaraj, P. Chaturvedi, H.J. Kim, D.S. Choi, *Mater. Lett.*, 283 (2021) 128737.
14. G. Liu, S. Zhang, X. Wei, S. Wang, Y. Yu, *Int. J. Electrochem. Sci.*, 11 (2016) 6799.

15. N. Zhou, H. Y. Wang, S. Q. Liu, G. Cao, Y. N. Liu, *Int. J. Electrochem. Sci.*, 8 (2013) 9149.
16. C. Sun, S. Rajasekhara, J.B. Goodenough, F. Zhou, *J. Am. Chem. Soc.*, 133 (2011) 2132.
17. Z. Ma, G. Shao, Y. Fan, G. Wang, J. Song, T. Liu, *ACS Appl Mater Interfaces*, 6 (2014) 9236.
18. Y.-P. Liang, C.-C. Li, W.-J. Chen, J.-T. Lee, *Electrochim. Acta*, 87 (2013) 763.
19. B. Wang, T.F. Liu, A.M. Liu, G.J. Liu, L. Wang, T.T. Gao, D.L. Wang, X.S. Zhao, *Adv Energy Mater*, 6 (2016) 1600426.
20. Y. Zhao, L. Peng, B. Liu, G. Yu, *Nano Lett.*, 14 (2014) 2849.
21. W. Kang, C. Zhao, R. Liu, F. Xu, Q. Shen, *CrystEngComm*, 14 (2012) 2245.
22. Y. Tao, Y. Cao, G. Hu, P. Chen, Z. Peng, K. Du, M. Jia, Y. Huang, J. Xia, L. Li, X. Xie, *J. Solid State Electrochem.*, 23 (2019) 2243
23. M. Wu, Z. Wang, L. Yuan, W. Zhang, X. Hu, Y. Huang, *Chin. Sci. Bull.*, 57 (2012) 4170.
24. R. Mei, X. Song, Y. Yang, Z. An, J. Zhang, *RCS Adv.*, 4 (2014) 5746.
25. M. Chen, F. Teng, G. Li, H. Shi, J. Wang, M. Xu, X. Ji, T. Lu, Y. Lv, S. Mho, *Ionics*, 18 (2012) 541.
26. H. Deng, S. Jin, L. Zhan, Y. Wang, W. Qiao, L. Ling, *J. Power Sources*, 220 (2012) 342.
27. Z. Zheng, W. K. Pang, X. Tang, D. Jia, Y. Huang, Z. Guo, *J. Alloys Compd.*, 640 (2015) 95.
28. Y. Wang, B. Zhu, Y. Wang, F. Wang, *Ceram. Int.*, 42 (2016) 10297.
29. F. Teng, S. Santhanagopalan, A. Asthana, X. Geng, S. Mho, R. S. Yassar, D. D. Meng, *J. Cryst. Growth*, 312 (2010) 3493.

© 2022 The Authors. Published by ESG ([www.electrochemsci.org](http://www.electrochemsci.org)). This article is an open access article distributed under the terms and conditions of the Creative Commons Attribution license (<http://creativecommons.org/licenses/by/4.0/>).